Improving Morphology and Performance of EPDM/Polypropylene/Clay Blends via PP-g-MA Compatibilization

Amir Hamzah Siregar*, Rizki Anggraini Nasution, and Risna Tanjung

Department of Chemistry, Faculty of Mathematics and Natural Sciences, Universitas Sumatera Utara, Jl. Bioteknologi No. 1, Medan 20155, Indonesia

* ***Corresponding author:***

email: amirhamzah@usu.ac.id

Received: September 16, 2025
Accepted: January 6, 2026

DOI: 10.22146/ijc.111264

Abstract: *This study investigates the effect of incorporating maleic anhydride-grafted polypropylene (PP-g-MA) as a compatibilizer on the morphological, thermal, and mechanical properties of EPDM/PP blends reinforced with clay powder for thermoplastic elastomer applications. PP-g-MA was prepared by refluxing in xylene, and EPDM/PP blends were prepared using the same procedure, incorporating PP-g-MA as a compatibilizer and clay powder as a filler at various loadings (0, 5, 10, 20, 30, 40 phr). The unmodified blends exhibited poor morphology due to phase incompatibility. In contrast, the addition of PP-g-MA significantly improved the dispersion of clay particles, resulting in a more homogeneous microstructure. The compatibilizer also enhanced mechanical performance, particularly tensile strength and elongation at break. Fourier-transform infrared (FTIR) spectroscopy confirmed the presence of hydrogen bonding between silica and PP-g-MA, while thermogravimetric analysis (TGA) indicated the highest thermal stability at 528.23 °C with a residue mass of 34.33%. These findings demonstrate the effectiveness of PP-g-MA in enhancing the overall performance of clay-reinforced EPDM/PP blends as thermoplastic elastomers.*

Keywords: *compatibilizer; clay powder; EPDM rubber; polypropylene; PP-g-MA*

■ INTRODUCTION

Polymer blends combine two or more structurally different polymers to create materials with enhanced properties. They are typically classified as plastic–plastic, plastic–rubber, and rubber–rubber blends, with plastic–rubber blends being the most widely used in industrial and commercial applications [1]. Thermoplastic vulcanizates (TPVs) are rubber–plastic blends that combine thermoplastic rigidity with elastomeric elasticity through dynamic vulcanization [2].

Polypropylene (PP) is one of the most widely used commodity plastics due to its low cost, light weight, ease of processing, flexibility, and chemical resistance. However, PP has several limitations, such as vulnerability to UV degradation, molding shrinkage, and low impact resistance. To address these drawbacks, various reinforcing agents—particularly elastomers—have been incorporated into the PP matrix [3]. Ethylene-propylene-diene monomer (EPDM) is known for its excellent weathering and thermal resistance, making it ideal for automotive applications. PP provides good tensile strength, which is beneficial for structural applications. The combination of EPDM and PP into a TPV can yield materials with improved overall properties [4].

However, the combination of EPDM and PP often results in inferior interfacial properties due to their differing polarities. Strategies frequently cited in the literature include increasing the polarity of components or incorporating compatibilizers, which act as mediators to strengthen interfacial bonding between existing phases [5]. Numerous studies have used maleic anhydride-grafted polypropylene (PP-g-MA) as an effective compatibilizer to improve interfacial adhesion in polymer blends [6]. Compatibilizers also enhance mechanical performance and improve the surface morphology of polymer blends [7].

The addition of clay has been shown to significantly improve the mechanical and thermal

properties of polymer composites and enhance their overall performance [8]. The silica in clay has a high surface area and a porous structure, enabling strong interactions with polymers. However, its dispersion within the polymer matrix is often hindered by agglomeration, which arises from polarity differences between hydrophilic silica and hydrophobic polymers. To improve compatibility, either compatibilizers or chemical surface modifications are used, thereby enhancing the performance of silica-reinforced polymer blends [9]. Compatibilizers typically function by binding one functional group to the polymer matrix and the other to the filler, thereby enhancing interfacial adhesion [5].

This study aims to evaluate the effectiveness of compatibilizers in addressing low compatibility issues and their potential to enhance the various material properties discussed previously. In this work, the compatibilizer PP-g-MA is synthesized, and an EPDM/PP/clay powder blend is prepared. The effect of the compatibilizer on the mechanical properties of the blend is analyzed, while the thermal properties and morphology are further investigated in the blend exhibiting the best mechanical performance.

■ EXPERIMENTAL SECTION

Materials

PP was supplied by PT Chandra Asri Petrochemical, Indonesia. EPDM rubber was supplied by PT Sumber Jaya Jakarta, Indonesia. Benzoyl peroxide and mercapto benzothiazole disulfide (MBTS) were purchased from Sigma-Aldrich, USA. Maleic anhydride, stearic acid, sulfur, and zinc oxide (ZnO) were provided by E. Merck, Germany. Xylene was supplied from PT Brataco Chemika (Bratachem), Indonesia. Clay was locally sourced from Wonosari Village, Tanjung Morawa, Medan, Indonesia.

Instrumentation

The clay powder was analyzed qualitatively by X-ray diffraction (XRD) using a Shimadzu XRD-6100 (Shimadzu, Japan) and quantitatively by X-ray fluorescence (XRF) using a Bruker S2 PUMA (Bruker, Germany). Mechanical and aging properties were assessed through tensile tests (ASTM D638-04, Tensilon RTF-1350, Dynatech, Japan) and impact tests (ASTM D256, Hung Ta-8041, Hung Ta, Taiwan). Fourier-transform infrared (FTIR) spectroscopy using a Shimadzu IR Prestige-21 (Shimadzu, Japan) was used to identify functional groups in PP-g-MA and EPDM/PP blends. Morphology was examined by scanning electron microscopy (SEM) using a Zeiss EVO MA10 (Zeiss, Germany), and thermal stability was evaluated by thermogravimetric analysis (TGA) using a Shimadzu DTG (Shimadzu, Japan).

Procedure

Sample preparation

A 1000-g sample of raw clay was thoroughly washed to remove surface impurities. The cleaned clay was then oven-dried at 105 °C for 3 h to eliminate residual moisture. After drying, the clay was ground and sieved through a 200-mesh sieve to obtain a fine powder. Subsequently, 500 g of the sieved clay powder were calcined at 900 °C for 3 h. The calcined clay was then sieved again through a 200-mesh sieve to ensure a uniform particle-size distribution.

Characterization of clay

XRD analysis. Calibration of the XRD began with adjustments to the current (XG control), cooling system, and shutter, followed by verification that the instrument was properly sealed. Approximately 2 mg of the sample was placed into the holder, and the operating voltage and X-ray wavelength were configured according to the instrument specifications. The resulting diffractogram was analyzed in terms of peak intensity and diffraction angle (2θ), and phase identification was performed using Joint Committee on Powder Diffraction Standards (JCPDS) reference patterns.

XRF analysis. The XRF instrument was powered on and calibrated before measurement. Upon completion of calibration, the sample holder automatically moved to the designated measurement position. The analysis was conducted at 14 kV and 90 μA for 5 min per sample. Analytical results were displayed on the DX-95 output interface.

Production of PP-g-MA

The blend was prepared via the solution-phase method using a reflux apparatus. A 100 phr PP was dissolved in xylene at 170 °C under continuous stirring.

Then, 3 phr maleic anhydride and 2 phr benzoyl peroxide were added to initiate grafting, and the mixture was stirred for 90 min. The resulting product was precipitated with methanol, dried, and subsequently analyzed using FTIR.

Production of EPDM/PP blends

The blend was prepared via the solution-phase method using a reflux apparatus. PP was dissolved in xylene at 170 °C, after which EPDM rubber, PP-g-MA, and clay powder were added. Paraffinic oil, stearic acid, and ZnO were then mixed into the blend for 4 min, followed by the addition of MBTS and sulfur, which were stirred for an additional 2 min. The homogeneous mixture was molded at 185 °C for 40 min according to ASTM D638 and D256 standards, and then cooled to room temperature. The compositional details of each material are presented in Table 1.

Composite characterization

Tensile strength analysis. Tensile strength was tested using a universal testing machine (Autograph type), in accordance with ASTM D638-22, operated at a crosshead speed of 50 mm/min with a maximum load capacity of 50,000 N. The Torsee electronic control system was stabilized for 1 h before testing. Each specimen was securely mounted in the machine's grips, and the testing parameters were configured. The procedure was repeated for each sample, and the resulting data were used to calculate the tensile strength and elongation at break using Eq. (1) and (2), respectively.

$$\sigma = \frac{F}{A_0} \quad (1)$$

$$\varepsilon = \frac{\Delta l}{L_0} \times 100\% \quad (2)$$

Aging analysis. Thermal aging resistance was evaluated by exposing the samples to 70 °C in a laboratory oven for 7 days. After thermal aging, tensile strength and elongation at break were re-evaluated to quantify the extent of mechanical property degradation.

Impact strength analysis. Rectangular test specimens measuring 60 mm in length were prepared in accordance with ASTM D256-24. Each specimen was positioned on the impact tester with a support span of 40 mm. The pendulum was raised to an angle of 150° and then released to strike the specimen. A preliminary trial without a specimen was conducted to account for energy losses due to friction and air resistance. Upon impact, the absorbed energy was recorded from the dial gauge.

FTIR analysis. The sample was prepared as a semi-solid mull and evenly spread between two NaCl plates. The assembled sample cell was placed in the sample holder and analyzed using FTIR, with absorbance recorded over the spectral range of 4000–500 cm^{-1}.

SEM analysis. The sample was coated with a thin gold–palladium layer using an Ion Sputter JFC-1100 under a vacuum pressure of 0.2 Torr. The coated sample was then irradiated with a 10 kV electron beam and imaged using SEM for approximately 4 min. The coating thickness was approximately 400 Å. Magnification was adjusted as needed to optimize microstructure observation.

TGA analysis. TGA was performed under a stepwise heating protocol, with mass changes recorded as a function of temperature. Thermal degradation behavior

Table 1. Formulation of EPDM/PP/clay powder blends

Ingredients	Role	Content (phr)
PP	Matrix phase	30
EPDM	Matrix phase	70
PP-g-MA	Compatibilizer	5
Clay powder	Filler	0, 5, 10, 20, 30, and 40
Paraffinic oil	Plasticizer	2
Stearic acid	Activator	1.5
ZnO	Activator	5
MBTS	Accelerator	1
Sulfur	Curing agent	1

and the corresponding decomposition temperature were identified from the thermogram.

■ RESULTS AND DISCUSSION

Characterization of Clay

XRD analysis

XRD analysis was conducted to determine the mineral phases present in the clay powder. The diffractogram in Fig. 1 exhibits prominent peaks at 2θ values of 20.82°, 26.64°, and 50.14°. These peaks correspond to the diffraction pattern of crystalline silica (SiO_2), as referenced in the JCPDS No. 47-0715, thereby confirming that SiO_2 is the principal component of the clay powder. This result is consistent with the findings of Minh et al. [10], who also reported SiO_2 diffraction peaks at 25.54° and 50.02°. The similarity in patterns provides further evidence that the clay powder is predominantly composed of SiO_2. In addition, the sharp peaks observed in the diffractogram indicate a high degree of crystallinity. Such crystallinity is particularly important, as it is generally associated with enhanced mechanical strength and thermal stability in composites reinforced with inorganic fillers.

XRF analysis

XRF analysis was conducted to quantitatively determine the oxide composition of the clay powder. As shown in Table 2, SiO_2 is the dominant component, accounting for 55.44% of the total composition. This high SiO_2 content is significant, as SiO_2 acts as the primary filler, enhancing stiffness, wear resistance, and thermal stability. Aluminum oxide (Al_2O_3), present at 27.05%, indicates the presence of aluminosilicate minerals such as kaolinite or illite, which further contribute to mechanical strength and heat resistance.

Iron oxide (Fe_2O_3) constitutes 11.18% of the composition and may influence both the color and thermal behavior of the clay. Potassium oxide (K_2O), detected at 2.30%, is commonly associated with clay minerals such as illite or mica. In addition to these major oxides, minor quantities (< 2%) of MgO, TiO_2, CaO, P_2O_5, MnO, Cl, ZrO_2, V_2O_5, SrO, Rb_2O, ZnO, CuO, Ga_2O_3, and Y_2O_3 were also identified. Although present in small amounts, these oxides can influence the composite material's chemical reactivity and interfacial adhesion.

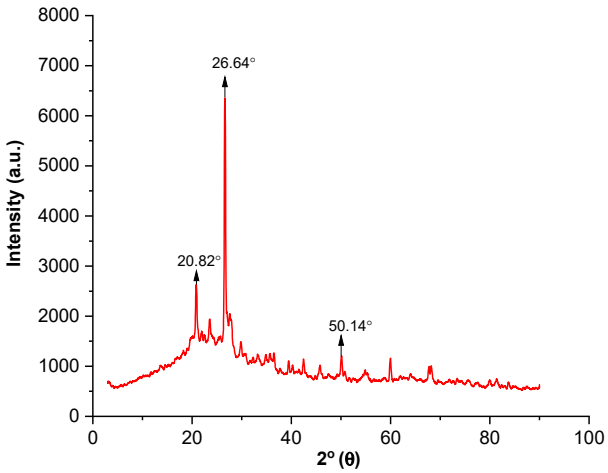

Fig 1. XRD of clay powder

Table 2. Chemical composition of clay powder

Compound	Concentration (wt.%)
Silicon oxide (SiO_2)	55.44 %
Aluminum oxide (Al_2O_3)	27.05 %
Iron oxide (Fe_2O_3)	11.18 %
Potassium oxide (K_2O)	2.30 %
Magnesium oxide (MgO)	1.57 %
Titanium oxide (TiO_2)	0.96 %
Calcium oxide (CaO)	0.89 %
Phosphorus oxide (P_2O_5)	0.24 %
Manganese oxide (MnO)	0.15 %
Chlorine (Cl)	0.05 %
Zirconium oxide (ZrO_2)	0.04 %
Vanadium oxide (V_2O_5)	0.03 %
Strontium oxide (SrO)	0.03 %
Rubidium oxide (Rb_2O)	0.02 %
Zinc oxide (ZnO)	0.01 %
Copper oxide (CuO)	0.01 %
Gallium oxide (Ga_2O_3)	0.01 %
Yttrium oxide (Y_2O_3)	0.01 %

Composite Characterization

Tensile strength analysis

According to the data presented in Table 3, the EPDM/PP blend without clay filler exhibits the lowest mechanical performance. This may be attributed to the low compatibility between PP and EPDM, arising from their differences in polarity, which leads to poor interfacial adhesion and reduced elongation at break.

In contrast, adding 10 phr clay powder filler and PP-g-MA to the blend results in a significant improvement

Table 3. Mechanical properties of EPDM/PP blends containing clay powder

EPDM:PP (phr)	Clay powder (phr)	Stress (MPa)	Strain (%)	Modulus Young (MPa)
70:30	0	7.523	7.75	97.08
	5	11.031	10.80	102.14
	10	14.021	13.44	104.32
	20	12.831	12.39	103.56
	30	10.698	10.88	98.33
	40	8.991	9.40	95.65

Table 4. Mechanical properties of EPDM/PP blends with clay powder after aging

EPDM:PP (phr)	Clay powder (phr)	Stress (MPa)	Strain (%)	Modulus Young (MPa)
70:30	0	7.091	8.49	83.53
	5	10.576	10.72	98.66
	10	13.243	11.54	114.76
	20	10.817	10.76	100.53
	30	10.544	10.10	104.40
	40	9.027	10.35	87.22

in mechanical properties. The addition of filler improves tensile strength due to strong interfacial interactions between the SiO_2 in the clay and the polymer matrix. The compatibilizer facilitates clay dispersion, thereby increasing the interfacial area and enhancing load transfer efficiency [8]. FTIR analysis supports these findings. The carbonyl groups in PP-g-MA can form interactions with the diene groups of the EPDM matrix and with hydroxyl groups on the SiO_2 surface.

However, adding clay powder filler beyond the optimal content results in a deterioration of mechanical properties. This decline in value results from the formation of agglomerates, which compromise the material's structural stability and consequently reduce its capacity for plastic deformation [11]. High filler loadings promote aggregate formation through strong filler–filler interactions, which can initiate cracking and degrade the mechanical performance of the blend. These aggregates may also reduce the compatibilization efficiency of PP-g-MA.

Aging analysis

The tensile test results after aging, as shown in Table 4, indicate a reduction in tensile strength for all samples. The EPDM/PP blend without clay powder filler exhibited the greatest reduction. In comparison, the EPDM/PP blend with 10 phr of clay powder filler also exhibited a decline in performance, but retained superior mechanical properties. Aging causes physical degradation, including increased hardness, softening, and tackiness, primarily due to oxidative reactions initiated by oxygen and ozone. These reactions are accelerated by environmental factors such as heat, ultraviolet (UV) radiation, humidity, and catalytic metal contaminants. During aging, oxidative reactions between free radicals and oxygen lead to chain scission and secondary cross-linking in the rubber matrix. These reactions increase stiffness and brittleness, depending on the type of rubber [12].

In the EPDM/PP blend without clay, weak interfacial bonding between the two polymer phases accelerates structural damage during aging. In contrast, in the EPDM/PP system reinforced with clay and compatibilized with PP-g-MA, well-dispersed SiO_2 particles act as barriers to oxygen and heat diffusion, thus reducing the degradation rate. The contributions of clay and PP-g-MA to enhancing aging resistance are particularly significant. Clay acts as a physical barrier that limits oxygen penetration and suppresses thermal degradation, while PP-g-MA improves interfacial adhesion between the polymer matrix and the filler, thereby reducing the formation of weak points that could serve as crack initiation sites. Optimum performance is achieved with 10 phr clay, at which the filler remains uniformly dispersed and provides maximum protection. However, beyond this concentration, filler agglomeration occurs, creating stress concentration sites that promote crack initiation and ultimately diminish the material's resistance to aging.

Impact strength analysis

The impact strength of EPDM/PP blends containing clay filler is presented in Fig. 2. The blend without filler exhibited the lowest impact strength. In contrast, the addition of 10 phr clay filler resulted in the highest value. Fig. 2 shows that the impact strength, measured using the Charpy method, increases initially but decreases at higher clay filler. The reduction in impact strength can be attributed to the increased size and concentration of

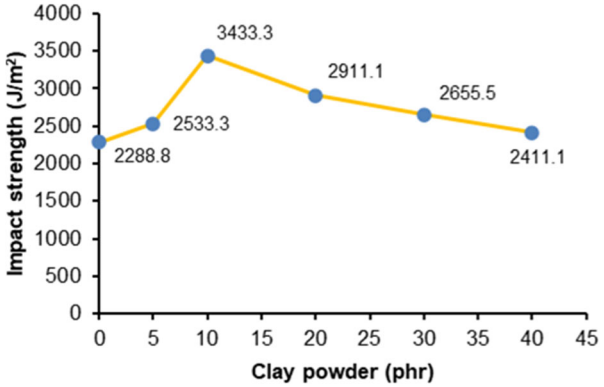

Fig 2. Impact strength of EPDM/PP/clay powder blends

filler particles, which induce stress concentrations at weak interfacial regions and result in inadequate reinforcement–matrix bonding, thereby diminishing the composite's capacity for energy absorption [13]. Polymer blends containing compatibilizers exhibit higher impact strength than those without. The incorporation of compatibilizers enhances interfacial bonding, thereby requiring more energy to separate the material phases. However, an increase in interfacial strength does not necessarily lead to a corresponding increase in impact strength [14].

When the clay content exceeds 10 phr, the impact strength progressively declines; for instance, at 40 phr, it decreases to 2411.1 J/m^2. This reduction is primarily attributed to two factors. First, the agglomeration of clay particles creates stress-concentration sites, facilitating crack initiation and propagation under impact loading. Second, the inherent brittleness of the inorganic filler restricts the polymer matrix's capacity for plastic deformation. Consequently, the composite absorbs less impact energy, resulting in premature failure during impact testing.

Although adding clay above 10 phr reduces impact strength due to particle agglomeration and the filler's inherent brittleness, the compatibilizer PP-g-MA plays a critical role in mitigating these adverse effects. PP-g-MA improves interfacial bonding between clay particles and the polymer matrix, enabling impact energy to be dissipated through matrix deformation rather than filler detachment. Furthermore, it helps prevent void formation around filler particles, which often act as crack initiation sites. Thus, even though impact strength declines at higher filler loadings, the presence of PP-g-MA ensures superior mechanical performance compared to composites without a compatibilizing agent.

FTIR analysis

FTIR analysis was performed to confirm the successful grafting of MA onto PP and to identify interactions among components in EPDM/PP blends reinforced with clay powder and compatibilized with PP-g-MA. The FTIR spectrum in Fig. 3(a) clearly distinguishes pure PP from PP-g-MA. In pure PP, characteristic absorption bands appear at 2922.2 cm^{-1} (asymmetric C–H stretching), 1453.7 cm^{-1} (CH_2 bending), and 1371.7 cm^{-1} (CH_3 bending), which are typical of the PP chain structure. In contrast, PP-g-MA exhibits new bands at 1714.5 cm^{-1}, corresponding to carbonyl (C=O) stretching of MA, and at 1162 cm^{-1}, associated with C–O

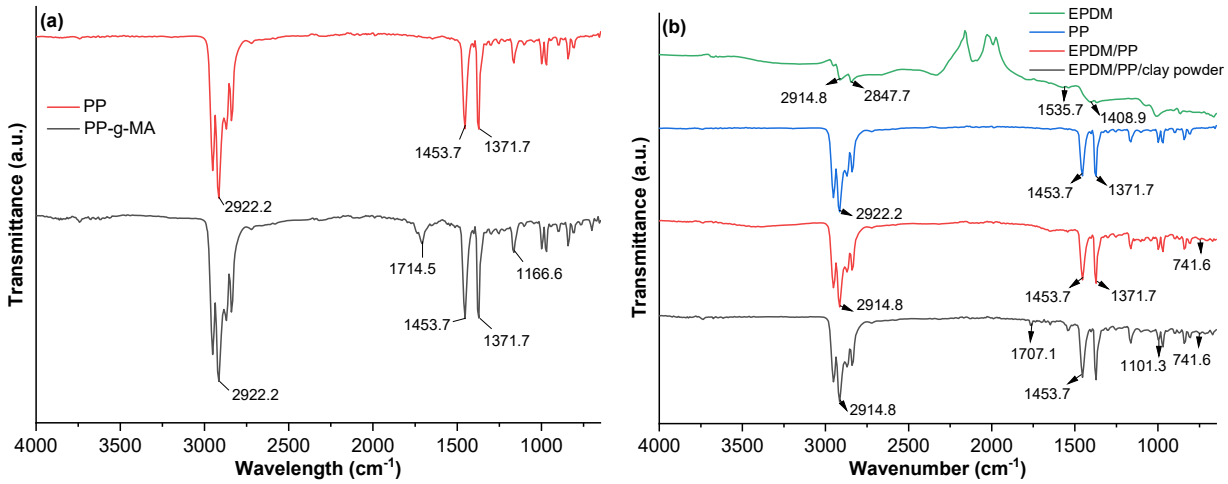

Fig 3. (a) FTIR spectra of PP-g-MA and (b) PP, EPDM, EPDM/PP, and EPDM/PP/clay powder

stretching. The observed absorption peak pattern corresponds to the characteristic features of MA. This observation indicates that PP-g-MA has been successfully grafted onto the PP matrix [15].

The FTIR spectra of EPDM, PP, EPDM/PP, and EPDM/PP/clay, presented in Fig. 3(b), display similar absorption bands corresponding to common polymer chain functional groups such as C–H, CH_2, and CH_3. However, in the EPDM/PP and EPDM/PP/clay blends, an additional band at 741.6 cm^{-1} emerges, which is attributed to the C–S bond formed during the sulfur vulcanization process. This observation indicates that vulcanization has occurred and has influenced the blend's structure. Furthermore, in the EPDM/PP/clay blend, an additional band at around 1110 cm^{-1} is observed, corresponding to Si–O stretching from the silica in the clay. This feature highlights the clay filler's contribution to the blend. Small shifts in wavenumber and variations in band intensity are also observed in the EPDM/PP and EPDM/PP/clay blends. These spectral changes suggest interactions among the components, particularly between the carbonyl groups of PP-g-MA and the hydroxyl groups of SiO_2. Such interactions confirm PP-g-MA's role as an effective compatibilizer, enhancing interfacial bonding between the polymer matrix and the clay particles.

SEM analysis

SEM analysis was performed to examine the surface morphology and clay particle distribution in EPDM/PP blends, both with and without the compatibilizer PP-g-MA. The observations clearly demonstrate the influence of clay and compatibilizer on the microstructure and homogeneity of the blends.

In the EPDM/PP sample without clay, as shown in Fig. 4(a) and 4(b), a distinct contrast is observed between the two phases. The lighter regions correspond to PP, while the darker regions represent EPDM. The morphology reveals that the EPDM phase is dispersed in relatively large domains and separated from the PP phase. This indicates weak interfacial bonding due to polarity differences between the polymers, leading to heterogeneity that adversely affects mechanical properties, particularly tensile strength and impact toughness.

In contrast, the EPDM/PP sample containing 10 phr clay and PP-g-MA, as shown in Fig. 4(c) and 4(d), exhibits a smoother surface with smaller EPDM domains in the uncompatibilized system [16]. Clay particles are uniformly dispersed in the polymer matrix, with no noticeable agglomeration. This indicates that PP-g-MA reduces interfacial tension and improves compatibility between the PP and EPDM phases, as well as between

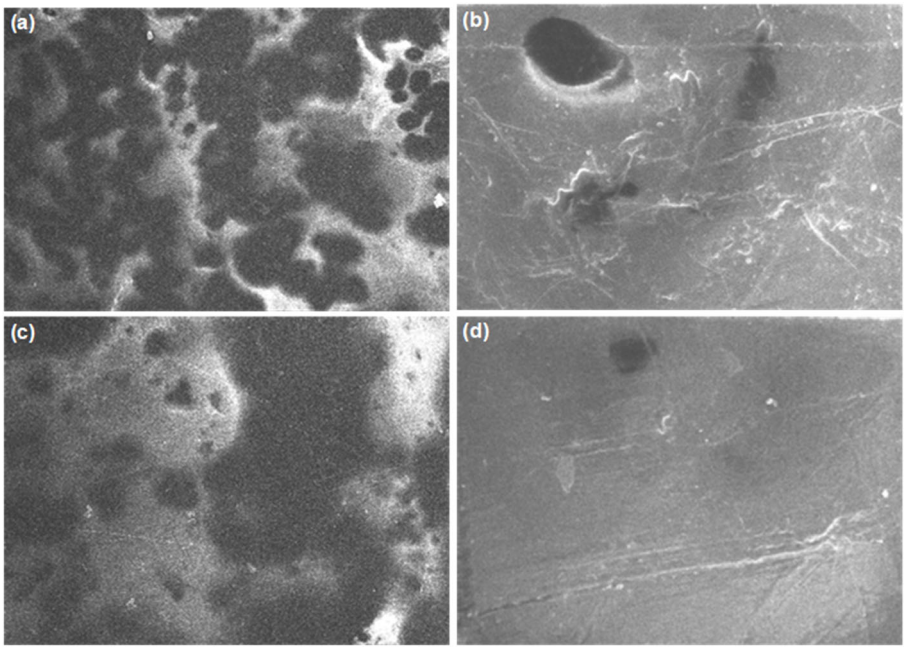

Fig 4. SEM images of EPDM/PP at (a) 60× and (b) 2000×, and EPDM/PP/clay (10 phr) at (c) 60× and (d) 2000×

the polymer matrix and the clay's silica surface [17]. The uniform filler dispersion facilitates efficient load transfer across phases, thereby enhancing tensile strength, modulus, and toughness.

This morphological improvement arises from chemical reactions between the anhydride groups of PP-g-MA and the hydroxyl (–OH) groups on the clay's silica surface via a nucleophilic substitution mechanism. These reactions form strong covalent bonds that suppress clay agglomeration and reduce the size of dispersed EPDM domains. As a result, the blend develops a more homogeneous microstructure, which supports improved mechanical properties and greater thermal stability of the composite.

TGA analysis

TGA was conducted to monitor weight changes as temperature increased. Fig. 5 presents the TGA curves for EPDM/PP and EPDM/PP blends containing 10 phr of clay powder. Three distinct degradation stages are observed: moisture evaporation, volatilization of low-molecular-weight compounds, and thermal decomposition of the polymer chains [18]. The TGA curves reveal three distinct stages of thermal degradation: dehydration (up to approximately 100 °C), thermal degradation of low-molecular-weight compounds (225–350 °C), and decomposition of the polymer backbone (400–500 °C). The TGA curves of both blends reveal an initial dehydration process occurring from room temperature to approximately 100 °C. This is followed by thermal degradation at 225–350 °C. The final stage corresponds to the decomposition of the primary polymer chains, occurring between 400 and 500 °C. For the EPDM/PP blend, decomposition occurs between 430.13 and 520.66 °C, resulting in approximately 71.76% weight loss. In contrast, the EPDM/PP/clay powder (10 phr) blend decomposes between 445.26 and 528.23 °C, with a corresponding weight loss of 65.67%.

The weight loss observed in the EPDM/PP blend is attributed to the release of trapped gases and moisture, as well as degradation by-products resulting from reactions involving hydrogen radicals and hydroxide species. The thermogram indicates that pyrolysis primarily results from

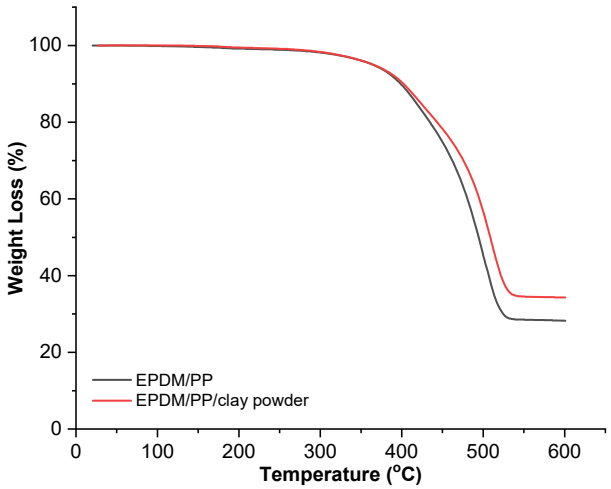

Fig 5. The thermogram of EPDM/PP and EPDM/PP/clay powder (10 phr) blends

the evaporation of volatile compounds generated by PP chain scission and the degradation of cross-links within the EPDM phase [19]. The incorporation of clay improved the thermal stability of the EPDM/PP blend, as the well-dispersed clay particles act as thermal insulators and barriers to the diffusion of volatile degradation products [8].

Proposed Mechanism of Interaction

Based on morphological analysis, a mechanism is proposed to elucidate the role of PP-g-MA as a compatibilizer in the EPDM/PP/clay/PP-g-MA blend. The maleic anhydride groups enhance interfacial adhesion by disrupting silica agglomerates and promoting a more uniform particle distribution. During the melt blending process, hydroxyl groups on the silica surface react with MA groups through a nucleophilic substitution reaction, as illustrated in Scheme 1. SiO_2 particles subsequently form chemical bonds with the polypropylene matrix via the PP-g-MA intermediary, thereby preventing agglomeration and aiding in the disintegration of large aggregates. In addition, hydrogen bonding may occur between carboxyl groups on the grafted PP-g-MA and hydroxyl groups on the SiO_2 surface. By reducing interfacial tension and improving adhesion, PP-g-MA enables the blend to better withstand mechanical stresses, as illustrated in Scheme 2 [20-21].

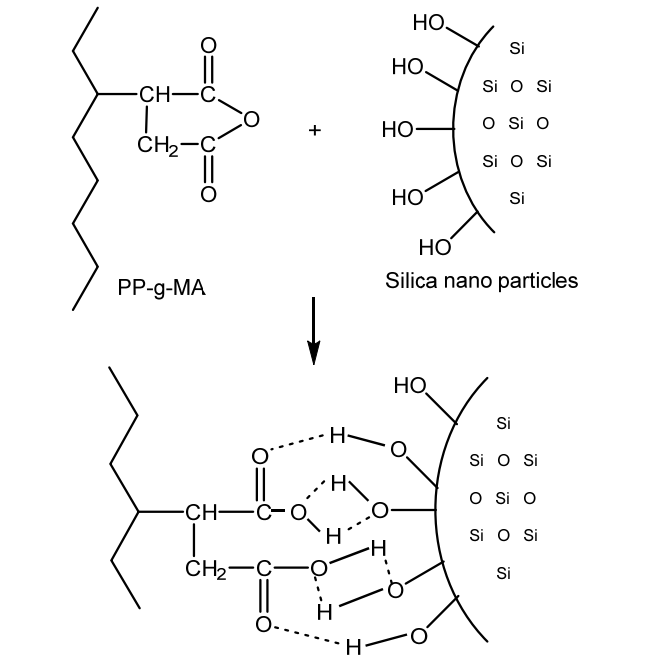

Scheme 1. Interaction between PP-g-MA and silica

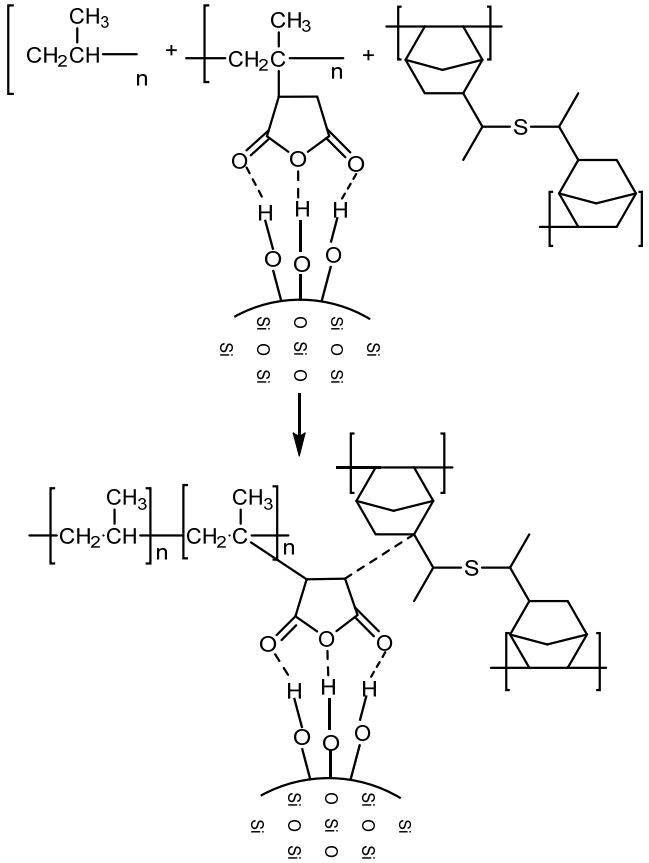

Scheme 2. Interaction between EPDM/PP/PP-g-MA/silica

■ CONCLUSION

This study demonstrates that incorporating maleic anhydride-grafted polypropylene (PP-g-MA) as a compatibilizer effectively enhances the performance of EPDM/PP blends reinforced with clay powder. The addition of PP-g-MA results in a more homogeneous morphology. PP-g-MA reduces interfacial tension and improves compatibility among PP, EPDM, and clay by forming robust covalent bonds with the clay's SiO_2 surface. This interaction promotes uniform filler dispersion, decreases agglomeration and domain size, and consequently improves the mechanical properties of the composite. The optimal composition was identified at 10 phr clay, achieving a tensile strength of 14.02 MPa and an elongation at break of 13.44%, indicating a substantial improvement over the unfilled blend. Thermal aging tests revealed that this composition retains good mechanical properties after-aging, suggesting resistance to thermal degradation. Furthermore, the highest impact strength was observed at 10 phr clay, with a decline at higher loadings attributed to particle agglomeration. FTIR results confirmed the successful grafting of PP-g-MA, as indicated by the appearance of characteristic MA peaks, and its interaction with hydroxyl groups on both SiO_2 and EPDM. TGA further demonstrated that the EPDM/PP blend with 10 phr clay exhibited the highest thermal stability, with a final degradation temperature of 528.23 °C and a residue mass of 34.33%. Overall, PP-g-MA significantly improves interfacial adhesion and improves the mechanical and thermal properties of EPDM/PP/clay composites, making it a promising compatibilizer for thermoplastic elastomer applications requiring high strength and thermal stability.

■ ACKNOWLEDGMENTS

The authors would like to express their gratitude to the heads of the Physical Chemistry Laboratory and the Polymer Chemistry Laboratory, Department of Chemistry, Faculty of Mathematics and Natural Sciences, Universitas Sumatera Utara, for their support of our research.

■ CONFLICT OF INTEREST

The authors have no conflicts of interest.

■ AUTHOR CONTRIBUTIONS

Amir Hamzah Siregar: Conceptualization, Methodology, Investigation, Writing – Review & Editing. Rizki Anggraini Nasution: Conceptualization, Methodology, Investigation, Writing – Original Draft Preparation, Writing – Review & Editing. Risna Tanjung: Investigation, Writing – Original Draft Preparation. All authors have read and agreed to the published version of the manuscript.

■ REFERENCES

[1] Panigrahi, H., Sreenath, P.R., Bhowmick, A.K., and Dinesh Kumar, K., 2019, Unique compatibilized thermoplastic elastomer from polypropylene and epichlorohydrin rubber, *Polymer*, 183, 121866.

[2] Oyarhoseini, H., Katbab, A.A., and Abdi, R., 2024, Dynamically vulcanized CNC-reinforced thermoplastic elastomer based on PP/EPDM: Morphology and mechanical properties control via interfacial compatibilization, *Polym. Eng. Sci.*, 64 (5), 2312–2323.

[3] Patra, P.K., Jaisingh, A., Goel, V., Kapur, G.S., and Nebhani, L., 2022, Crystallization kinetics of compatibilized blends of polypropylene and polyethylenimine, *J. Therm. Anal. Calorim.*, 147 (12), 6689–6699.

[4] Bhattacharya, A.B., Raju, A.T., Chatterjee, T., and Naskar, K., 2020, Development and characterizations of ultra-high molecular weight EPDM/PP based TPV nanocomposites for automotive applications, *Polym. Compos.*, 41 (12), 4950–4962.

[5] Gangwani, P., Kalin, M., and Emami, N., 2023, Does a compatibilizer enhance the properties of carbon fiber-reinforced composites?, *Polymers*, 15 (23), 4608.

[6] Panigrahi, H., Sreenath, P.R., and Kotnees, D.K., 2020, Unique compatibilized thermoplastic elastomer with high strength and remarkable ductility: effect of multiple point interactions within a rubber-plastic blend, *ACS Omega*, 5 (22), 12789–12808.

[7] Durmaz, B.U., and Aytac, A., 2019, Characterization of carbon fiber-reinforced poly(phenylene sulfide) composites prepared with various compatibilizers, *J. Compos. Mater.*, 54 (1), 89–100.

[8] Nakhaei, M.R., Mostafapour, A., Dubois, C., Naderi, G., and Reza Ghoreishy, M.H., 2019, Study of morphology and mechanical properties of PP/EPDM/clay nanocomposites prepared using twin-screw extruder and friction stir process, *Polym. Compos.*, 40 (8), 3306–3314.

[9] Mokhtari Dizaji, S., Katbab, A.A., and Hajibabazadeh, S., 2023, Role of interfacial compatibilizer and functionality of rubber phase on micromorphology development and mechanical properties of PP/EPDM/nanosilica ternary nanocomposite, *Polym. Bull.*, 80 (2), 1353–1368.

[10] Minh, V.C., Huy, N.N., Thi, T.N., and Nguyen, L.T.L., 2025, Adsorption characteristics of coconut husk biochar for organics in water, *Indones. J. Chem.*, 25 (3), 730–743.

[11] Siraj, S., Al-Marzouqi, A.H., Iqbal, M.Z., and Ahmed, W., 2022, Impact of micro silica filler particle size on mechanical properties of polymeric based composite material, *Polymers*, 14 (22), 4830.

[12] Zhou, B., Liu, W., Huang, Y., Luo, J., and Yin, B., 2025, Effect of thermo-oxidative, ultraviolet and ozone aging on mechanical property degradation of carbon black-filled rubber materials, *Buildings*, 15 (15), 2705.

[13] Ramesh, M., Rajeshkumar, L.N., Srinivasan, N., Kumar, D.V., and Balaji, D., 2022, Influence of filler material on properties of fiber-reinforced polymer composites: A review, *e-Polym.*, 22 (1), 898–916.

[14] Savas, L.A., Tayfun, U., and Dogan, M., 2016, The use of polyethylene copolymers as compatibilizers in carbon fiber reinforced high density polyethylene composites, *Compos. B Eng.*, 99, 188–195.

[15] Chabira, A.S., Bouremel, C., Sakri, A., and Boutarfaia, A., 2022, Synthesis and characterization of biocomposites based polypropylene/thermoplastic starch-reinforced with natural *Stipa tenacissima* fibers and PP-g-MA, *Metall. Mater. Eng.*, 28 (3), 487–501.

[16] Azizli, M.J., Barghamadi, M., Rezaeeparto, K., and Parham, S., 2022, Improvement of mechanical, morphological and thermal properties on PP-enriched graphene oxide/PP-g-MA/EPDM blend compatibilized: PP-g-MA compatibilizer and graphene oxide nanofiller role, *J. Polym. Res.*, 29 (8), 322.

[17] Zoukrami, F., Haddaoui, N., Sclavons, M., Devaux, J., and Vanzeveren, C., 2018, Rheological properties and thermal stability of compatibilized polypropylene/untreated silica composites prepared by water injection extrusion process, *Polym. Bull.*, 75 (12), 5551–5566.

[18] Siregar, A.H., Warman, A., Harahap, M., Nainggolan, G., Dellyansyah, D., and Gea, S., 2021, Preparation of biodegradable and low-cost lignin-based PVOH carbon fibers prepared by electrospinning, *Indones. J. Chem.*, 21 (6), 1463–1470.

[19] Sarfraz, M., ur Rehman, Z., and Ba-Shammakh, M., 2019, Pursuit of electroconducting thermoplastic vulcanizates: Activated charcoal-filled polypropylene/ethylene–propylene–diene monomer blends with upgraded electrical, mechanical and thermal properties, *Polym. Bull.*, 76 (4), 2005–2020.

[20] Bansod, N.D., Kapgate, B.P., Maji, P.K., Bandyopadhyay, A., and Das, C., 2019, Functionalization of EPDM rubber toward better silica dispersion and reinforcement, *Rubber Chem. Technol.*, 92 (2), 219–236.

[21] Ibrahim, M.A.H., Hassan, A., Wahit, M.U., Hasan, M., and Mokhtar, M., 2016, Mechanical properties and morphology of polypropylene/poly (acrylonitrile-butadiene-styrene) nanocomposites: Effect of compatibilizer and montmorillonite content, *J. Elastomers Plast.*, 49 (3), 209–225.